STRUCTURAL BIOLOGY COMMUNICATIONS

ISSN 2053-230X

Crystal structure of thermostable acetaldehyde dehydrogenase from the hyperthermophilic archaeon *Sulfolobus tokodaii*

Shohei Mine,[a] Makoto Nakabayashi[b] and Kazuhiko Ishikawa[a,c]*

[a]Biomedical Research Institute, National Institute of Advanced Industrial Science and Technology (AIST), 1-8-31 Midorigaoka, Ikeda, Osaka 563-8577, Japan, [b]Faculty of Pharmacy, Osaka Ohtani University, 3-11-1 Nishikiori-kita, Tondabayashi, Osaka 584-8540, Japan, and [c]Rare Sugar and Enzyme Research, Dep. I, R&D, Matsutani Chemical Industry Co. Ltd, 5-3 Kitaitami, Itami City, Hyogo 664-8508, Japan. *Correspondence e-mail: kazuhiko-ishikawa@matsutani.co.jp

Received 15 February 2023
Accepted 22 May 2023

Edited by A. Nakagawa, Osaka University, Japan

Keywords: thermostability; acetaldehyde dehydrogenase; aldehydes; archaea; *Sulfolobus tokodaii*.

PDB reference: acetaldehyde dehydrogenase, 8hap

Supporting information: this article has supporting information at journals.iucr.org/f

Aldehyde dehydrogenase (ALDH) is widely distributed in nature and its characteristics have been examined. ALDH plays an important role in aldehyde detoxification. Sources of aldehydes include incomplete combustion and emissions from paints, linoleum and varnishes in the living environment. Acetaldehyde is also considered to be carcinogenic and toxic. Thermostable ALDH from the hyperthermophilic archaeon *Sulfolobus tokodaii* exhibits high activity towards acetaldehyde and has potential applications as a biosensor for acetaldehyde. Thermostable ALDH displays a unique and wide adaptability. Therefore, its crystal structure can provide new insights into the catalytic mechanism and potential applications of ALDHs. However, a crystal structure of a thermostable ALDH exhibiting high activity towards acetaldehyde has not been reported to date. In this study, crystals of recombinant thermostable ALDH from *S. tokodaii* were prepared and the crystal structure of its holo form was determined. A crystal of the enzyme was prepared and its structure in complex with NADP was determined at a resolution of 2.2 Å. This structural analysis may facilitate further studies on catalytic mechanisms and applications.

1. Introduction

Aldehyde dehydrogenase (EC 1.2.1.*x*; ALDH) is widely distributed in the three domains of life: eukarya, bacteria and archaea. ALDH represents an important mechanism for aldehyde detoxification with reduction of the coenzyme NAD or NADP (Perozich *et al.*, 1999). Based on sequence similarity and substrate specificity, ALDHs can be classified into 81 categories (https://enzyme.expasy.org/; Bairoch, 2000), with different types of ALDH having distinct catalytic properties. Some ALDHs with distinctive catalytic properties have particular value in therapeutics and biotechnology (Kimura *et al.*, 2019; Wang *et al.*, 2020; Demkiv *et al.*, 2008; Zhang *et al.*, 2022). Although ALDH has been extensively studied in eukarya and bacteria, the structure and biochemical properties of archaeal ALDHs have not been reported in detail. As enzymes in archaea usually display unique catalytic properties, such as high catalytic efficiency and adaptability to the environment (Ishikawa *et al.*, 2001; Kim & Ishikawa, 2011; Kataoka & Ishikawa, 2014), characterization of ALDHs from archaea can provide new insights into the their catalytic mechanisms and potential applications. In particular, the thermostabilities of these enzyme are highly informative. ALDH from the hyperthermophilic archaeon *Sulfolobus*

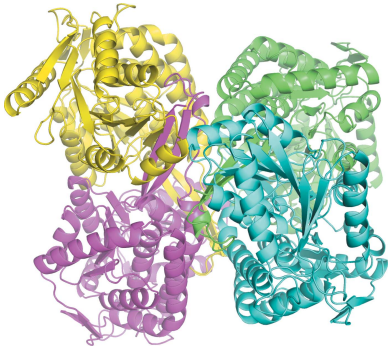

Table 1
Macromolecule-production information.

Source organism	*Sulfolobus tokaidaii*
DNA source	Synthetic DNA
Cloning vector	pCold II
Expression vector	pCold II
Expression host	*Escherichia coli* BL21 (DE3)
Complete amino-acid sequence of the construct produced†	**MNHKVHHHHHH**MSEVIEIKSPSNLKVIGTV KRMSKDEVRGEIEEAYKGFETISRMPLYK RTAILRKVSEILEREQERLARLLAMEAGK PIKDSRVEVMRASRLFRQAAEEAAIVLEG KNYRVDAYEYPPGNENRIVISTREPIGVV TAILPFNFPINSFAHKVAPAIAVGNSVVV KPSISTPLSAIEMKKILVEAGLPDSAVRI VTGYSNEIGDELITHPLVGLITLTGSTQT GLAIASKAVSLGKRIIMELGGSDPIIVLE DANIDRASSIAVRARYEYAGQNCNAGKRI IVREEIYDKFVKAFKEKVKALKVGDPLDE STDIGPVINQESVEKLNKALEDAQSKGGN VEVLNKGPETGYFFPLSLVTNPSLDMLVL KTEIFGPIAPIVSVKSDEEAINIANSTEY GLQSAIFSNDVNRALKIAKELKFGAIIIN DSTRLRWDSLPFGGFKKTGIGREGVRDTM LEMTENKLIAITLL

† The His tag is shown in bold.

tokodaii (ALDH*St*) has been reported to exhibit high activity towards acetaldehyde (Liu *et al.*, 2013) and succinate semialdehyde (Ito *et al.*, 2013). Furthermore, this enzyme is the most thermostable ALDH reported to date and this unique property is potentially beneficial in the fields of biosensors, biotechnology and biomedicine. Formaldehyde and acetaldehyde are well known mutagens and carcinogens. Thermostable ALDHs can be used as biosensors for the detection of these aldehydes. A biosensor for formaldehyde has been developed using a thermostable ALDH which exhibits high activity towards formaldehyde (Monkawa *et al.*, 2015). However, there have been no reports of a biosensor for acetaldehyde using a thermostable ALDH. Crystallographic structure analysis of a thermostable ALDH that exhibits high activity towards acetaldehyde may be highly informative. Therefore, in this study, we report the crystallization and crystal structure of the thermostable ALDH*St*.

2. Materials and methods

2.1. Production of ALDH*St*

An ALDH exhibiting high activity towards acetaldehyde was reported in the hyperthermophilic archaeon *S. tokodaii* (Liu *et al.*, 2013). We prepared recombinant ALDH*St* using a previously described method (Liu *et al.*, 2013). The open reading frame (ORF) of the enzyme was chemically synthesized using a codon optimized for *Escherichia coli*. A pCold II vector (Takara Bio, Shiga, Japan) harboring the ORF was constructed using polymerase chain reaction. The constructed plasmids were introduced into *E. coli* strain BL21(DE3) for recombinant protein expression. The transformant was cultured in Luria–Bertani broth containing 100 µg ml^{-1} ampicillin sodium at 37°C until the OD_{600} reached 0.6. 0.1 m*M* isopropyl β-D-1-thiogalactopyranoside was added, followed by further cultivation at 15°C for 21 h. The cells were harvested by centrifugation (5000*g*, 15 min, 4°C) and then homogenized by ultrasonication in 20 m*M* Tris–HCl pH 8.0; the homogenates were then heated at 80°C for 30 min and centrifuged (15 000*g*, 30 min, 4°C). The resulting supernatant was applied onto a HisTrap HP column (GE Healthcare, Buckinghamshire, United Kingdom) pre-equilibrated with 20 m*M* Tris–HCl pH 8.0; the column was then washed with 20 m*M* imidazole followed by elution with 500 m*M* imidazole. The peak fraction was subjected to gel-filtration chromatography (HiLoad 26/600 Superdex 200 pg column). The purity and molecular weight of the protein samples were analyzed using sodium dodecyl sulfate–polyacrylamide gel electrophoresis (SDS–PAGE). The protein concentration was determined using the Bradford method against a bovine serum albumin standard. Macromolecule-production information is summarized in Table 1.

Table 2
Crystallization.

Method	Vapor diffusion
Plate type	Sitting drop
Temperature (K)	293
Protein concentration (mg ml^{-1})	20
Buffer composition of protein solution	20 m*M* Tris–HCl pH 8.0
Composition of reservoir solution	0.1 *M* sodium phosphate dibasic/citric acid pH 4.2, 0.2 *M* sodium chloride, 10%(*w*/*v*) PEG 3000
Volume and ratio of drop	1 µl; 1:1 protein:reservoir solution
Volume of reservoir (µl)	60

2.2. Crystallization

The purified enzyme was concentrated to 20 mg ml^{-1} and dialyzed against 20 m*M* Tris–HCl pH 7.5 using an Amicon Centricon YM-10 (Millipore, Billerica, Massachusetts, USA). Enzyme crystals were obtained using the sitting-drop vapor-diffusion method in a 96-well plate (Corning, New York, USA) at 293 K (Table 2). Crystals with good diffraction properties were obtained in a droplet consisting of 0.5 µl protein solution and 0.5 µl reservoir solution [100 m*M* sodium phosphate dibasic/citric acid pH 4.2, 200 m*M* sodium chloride, 10%(*v*/*v*) polyethylene glycol (PEG) 3000] equilibrated against 60 µl reservoir solution.

2.3. Data collection and processing

The selected crystals were harvested and immersed in a cryoprotectant solution consisting of 25%(*v*/*v*) glycerol in the mother liquor. The soaked crystals were collected using a CryoLoop (Hampton Research, Aliso Viejo, California, USA) and immediately flash-cooled under a stream of nitrogen gas at 100 K. X-ray diffraction data were collected from a single crystal using an MX-300HE CCD detector (Rayonix, Evanston, Illinois, USA) on the BL44XU beamline at SPring-8, Hyogo, Japan (Table 3). A diffraction data set was collected to 2.2 Å resolution at a wavelength of 0.9 Å. The distance between the crystal and the detector was 300 mm. The crystal was rotated by 180° with an oscillation angle of 1.0° per frame. The diffraction data were merged, indexed, integrated and

Table 3
Data collection and processing.

Values in parentheses are for the outer shell.

Diffraction source	BL44XU, SPring-8
Wavelength (Å)	0.9000
Detector	Dectris EIGER 16M
Total rotation range (°)	180
Oscillation range (°)	1.0
Space group	*C*2
a, *b*, *c* (Å)	164.07, 75.36, 105.31
α, β, γ (°)	90.00, 124.64, 90.00
Resolution range (Å)	46.55–2.20 (2.32–2.20)
Total No. of reflections	182293 (25041)
No. of unique reflections	53563 (7698)
Completeness (%)	99.0 (97.7)
Multiplicity	3.4 (3.3)
Mn(*I*) half-set correlation ($CC_{1/2}$)	0.997 (0.794)
$\langle I/\sigma(I)\rangle$	9.9 (2.3)
$R_{r.i.m.}$	0.104 (0.704)
$R_{p.i.m.}$	0.056 (0.383)
Overall *B* factor from the Wilson plot (Å^2)	30.699

Table 4
Structure refinement.

Resolution range (Å)	46.60–2.20 (2.254–2.197)
Completeness (%)	98.99 (95.61)
σ Cutoff	$F > 0.000\sigma(F)$
No. of reflections, working set	48165 (3646)
No. of reflections, test set	2699 (184)
Final R_{cryst}	0.168 (0.152)
Final R_{free}	0.214 (0.231)
No. of non-H atoms	
Total	7515
Protein	7176
Ligands	70
Ions	2
Solvent	267
R.m.s. deviations	
Bond lengths (Å)	0.009
Angles (°)	1.560
Average *B* factors (Å^2)	
Protein	38.68
Ligands	52.36
Ions	34.89
Solvent	48.11
Ramachandran plot	
Most favored (%)	97.7
Allowed (%)	2.3
Outliers (%)	0.0

scaled using programs in the *HKL*-2000 package (Otwinowski & Minor, 1997).

2.4. Structure solution and refinement

The structure was solved by molecular replacement with *MOLREP* (Vagin & Teplyakov, 2010) in the *CCP*4 package using the structure of ALDH (PDB entry 3pqa; New York Structural Genomics Research Consortium, unpublished work) as a search model. Structural model building was performed using *Coot* (Emsley *et al.*, 2010). The structure was refined using *REFMAC*5 (Murshudov *et al.*, 2011) (Table 4). Water molecules were introduced at peaks greater than 3.0σ in the difference Fourier map that fulfilled reasonable interactions with the protein model. The Ramachandran plot of the final structure was validated using *RAMPAGE* (Lovell *et al.*, 2003). Molecular-graphics images were generated using *PyMOL* (http://www.pymol.org).

3. Results and discussion

3.1. Overall structure of ALDH*St*

Recombinant ALDH*St* was prepared as a homotetramer, and crystals with good diffraction properties were obtained using the method described above. The average dimensions of the crystal were approximately 0.7 × 0.5 × 0.3 mm after one week. Diffraction data were collected to a resolution of 2.2 Å.

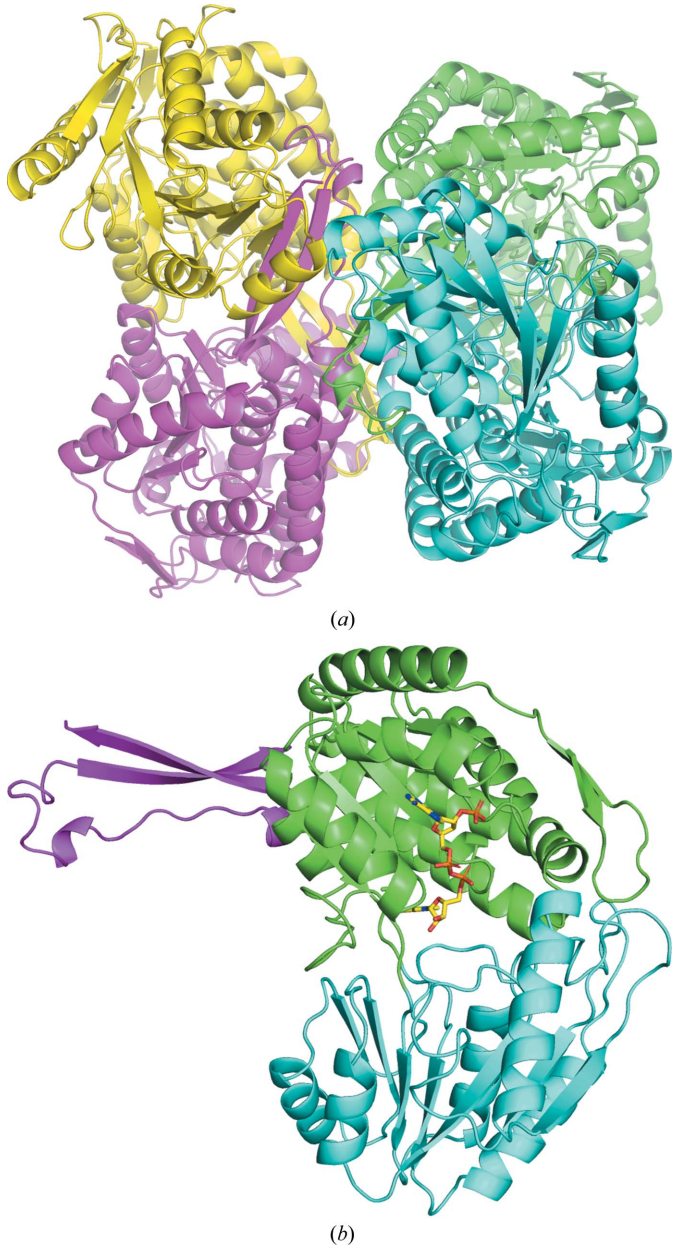

Figure 1
Ribbon diagram of the ALDH*St* homotetramer and monomer structures. (*a*) The homotetramer is a dimer of dimers (yellow/magenta and cyan/green) with crystallographic 222 symmetry. (*b*) Structure of the monomer subunit. The cofactor-binding domain, catalytic domain and oligomerization domain are shown in green, cyan and magenta, respectively. NADP is shown as a yellow stick model.

The data set comprised 182 293 measurements and 53 563 unique reflections. The results of data collection and analysis revealed that the crystal belonged to space group *C*2, with unit-cell parameters $a = 164.07$, $b = 75.36$, $c = 105.31$ Å, $\beta = 124.64^\circ$. The data-collection statistics are summarized in Table 3. The presence of a dimer in the asymmetric unit yields a crystal volume per protein mass (V_M) of 2.57 Å^3 Da^{-1} and a solvent content of 52.26%(*v*/*v*) (Matthews *et al.*, 1968). The structure was determined by the molecular-replacement method using previous structural data for ALDH (PDB entry 3pqa; glyceraldehyde-3-phosphate dehydrogenase GapN from *Methanocaldococcus jannaschii*; New York Structural Genomics Research Consortium, unpublished work). The ALDH*St* crystal was prepared without the coenzyme NADP; however, an omit $F_o - F_c$ electron-density map for NADP was contoured near the active site. Superimposition of ALDH*St* and the holo form of ALDH from the archaeon *Pyrobaculum* sp. 0.1860 (ALDH*Ps*) in complex with NADP (PDB entry 5ek6) revealed the NADP-binding site of ALDH*St*. The model of NADP identified in PDB entry 5ek6 can be superimposed

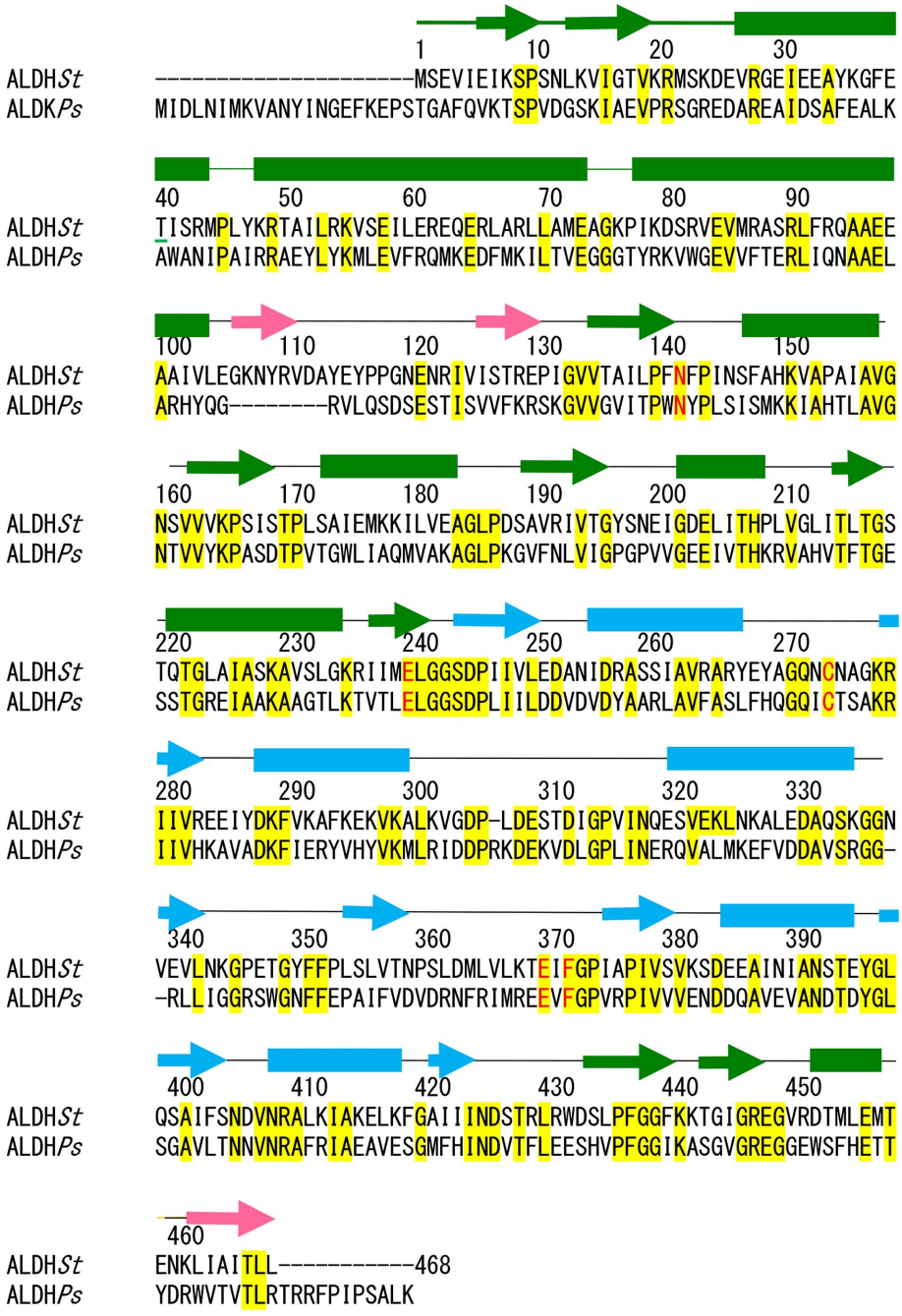

Figure 2
Sequence alignment of ALDH*St* and ALDH*Ps*. Identical residues are shown on a yellow background and conserved active-site residues are shown in red. β-Strands and α-helices are shown as colored arrows and boxes, respectively. The cofactor-binding, catalytic and oligomerization domains are indicated in green, cyan and magenta, respectively.

onto the structural model of ALDH*St*. After refinement, the structures of the adenine moiety, the pyrophosphate group and both ribose units of NADP were ordered in ALDH*St*. NADP appeared to be derived from the *E. coli* strain BL21(DE3) host cells. A similar phenomenon has previously been reported by Ishikawa *et al.* (2007). The structure was determined to 2.2 Å resolution and the *R* factors were estimated to be R_{work} = 16.8% and R_{free} = 21.4% (Table 4). The two molecules were very similar in the crystal structure. A noncrystallographic twofold axis of symmetry that relates two molecules was observed. The crystal structure exhibits a homotetrameric structure with crystallographic and noncrystallographic 222 symmetry. These results suggest that the biological assembly of ALDH*St* is a homotetramer (Fig. 1*a*). Each monomer of the final model contains 465 amino-acid residues. The obtained coordinates and structural factors have been deposited in the Protein Data Bank as entry 8hap. The overall structure of ALDH*St* adopts the canonical ALDH-fold structure as in bacteria and humans. The monomer is composed of three domains: the cofactor-binding domain (residues 1–103, 132–243 and 431–458), catalytic domain (residues 244–430) and oligomerization domain (residues

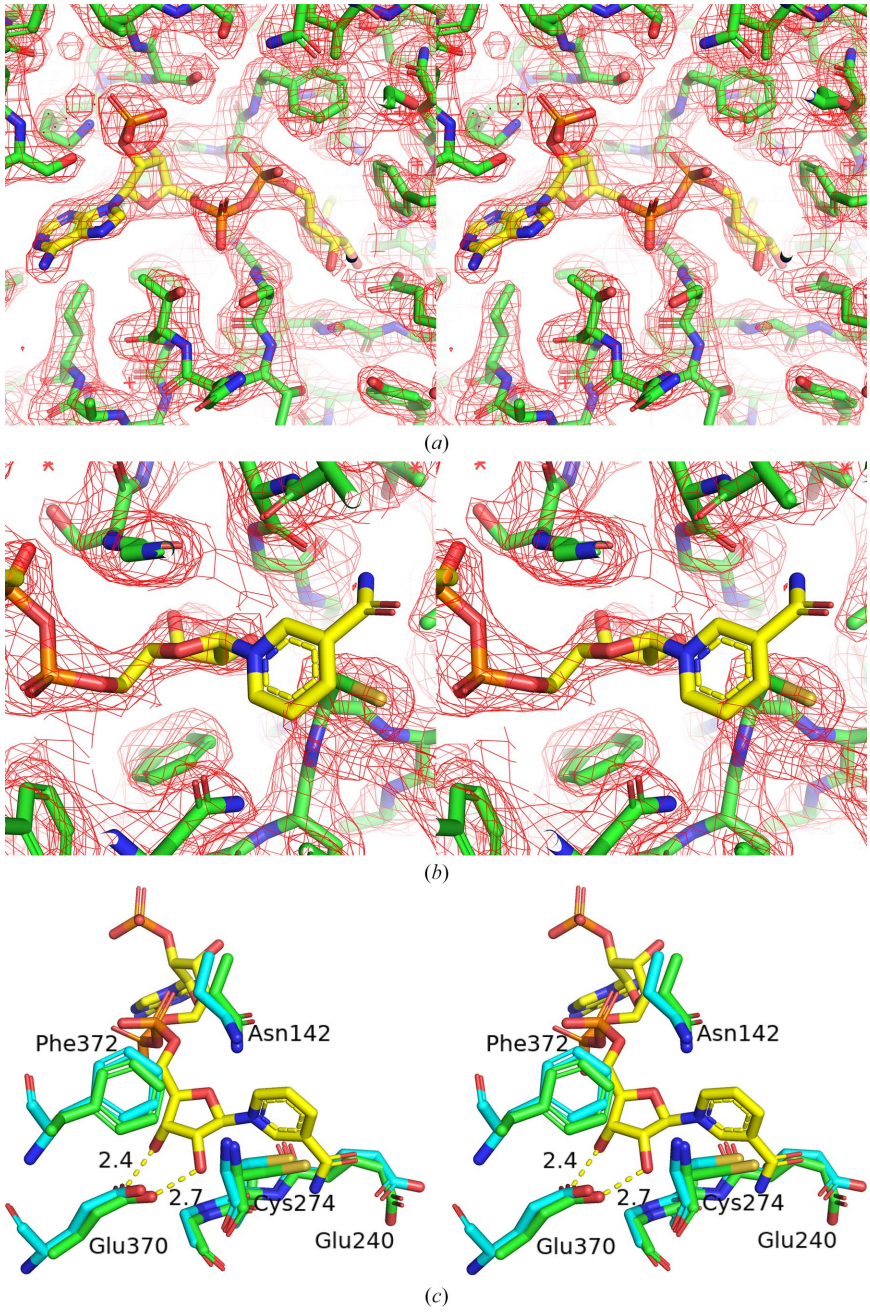

Figure 3
Cross-eyed stereo figures of the conformation of active-site residues in ALDH*St*. (*a*, *b*) The coenzyme (NADP) is shown in yellow. The $2F_o - F_c$ electron-density map around NADP is contoured at 1σ and colored red. (*c*) The catalytic residues Asn142, Glu240, Cys274, Glu370 and Phe372 in ALDH*St* are shown in green. Their corresponding residues in ALDH*Ps* (PDB entry 5ek6) are shown in cyan. Hydrogen bonds are shown as dashed lines.

104–131 and 459–467) are indicated in green, cyan and magenta, respectively (Figs. 1*b* and 2). Further, ALDH*St* exhibits considerable structural and sequence similarity (31.1% sequence identity) to ALDH*Ps* (optimum temperature of 75°C; Fig. 2; Liu *et al.*, 2013; Bezsudnova *et al.*, 2016). ALDH*Ps* has a long tail at the C-terminus, which strengthens the dimeric structure of the enzyme (Fig. 2). The absence of a similar tail in ALDH*St* (optimum temperature of 80°C; Liu *et al.*, 2013) indicates that the tail is not an important factor for the thermostability of ALDH*St*.

3.2. Structure of the active site

An omit $F_o - F_c$ electron-density map for NADP was contoured near the active site. After refinement, the structures of the adenine moiety, pyrophosphate group and both ribose units of NADP were well ordered in ALDH*St* (Fig. 3*a*). A $2F_o - F_c$ electron-density map for the nicotinamide moiety of NADP was not observed (Fig. 3*b*). The active-site conformation of ALDH*St* is homologous to that of ALDH*Ps* (Bezsudnova *et al.*, 2016). In the apo form of ALDH*Ps*, a hydrogen bond was observed between Glu253 and Gly255 (Bezsudnova *et al.*, 2016). However, no hydrogen bond was observed between Glu240 and Gly242 (corresponding to Glu253 and Gly255, respectively, in ALDH*Ps*). These results indicate that the structure of ALDH*St* in this study is a holo form complexed with NADP. Focusing on the cofactor-binding site, the catalytic side chains of Glu253 and Cys287 in ALDH*Ps* (Bezsudnova *et al.*, 2016) were found to be well conserved in the corresponding residues, Glu240 and Cys274, in ALDH*St* (Fig. 3*c*). A comparison of previously characterized ALDH*Ps* active sites (Liu *et al.*, 2013; Bezsudnova *et al.*, 2016) suggests that the catalytic side chain of Cys274 is directed away from the NADP-binding site (Fig. 3*c*) and attacks the aldehyde group of the substrate in the first step of the enzyme reaction. Secondly, a hydride-transfer reaction from the hemithioacetal intermediate to the nicotinamide ring of NADP has been proposed. Most residues around the active site of ALDH*Ps* are also well conserved in ALDH*St*. In this study, the $2F_o - F_c$ electron-density map around the nicotinamide moiety in NADP was weak (Fig. 3*b*). The nicotinamide moiety seems to be flexible in ALDH*St*, similar to that in ALDH*Ps* (Bezsudnova *et al.*, 2016). In the catalytic process, the nicotinamide ribose of NADP in the 'hydride-transfer' conformation was observed in ALDH*Ps* (Bezsudnova *et al.*, 2016). The structural similarity of the active site between ALDH*St* and ALDH*Ps* means that ALDH*St* also has the 'hydride-transfer' conformation (Fig. 3*c*); the nicotinamide ribose of NADP is stabilized by a hydrogen bond between the O2D atom of NADP and Glu370, as well as by a stacking interaction between the nicotinamide ribose and Phe372. These residues correspond to Glu382 and Phe384 in ALDH*Ps*, respectively. An omit $F_o - F_c$ electron-density map for ligands was observed between the side chains of Asn142 and Cys274 (Fig. 4). This space appeared to be the binding-site cleft for the substrate. This structural feature has also been observed in ALDH*Ps* (Bezsudnova *et al.*, 2016) and in ALDH from *Streptococcus mutans* (Cobessi *et al.*, 2000). Therefore, we propose the involvement of the amide group of the side chain of Asn142 in an oxyanion hole (Fig. 4) to stabilize the reaction intermediate, as suggested previously (Cobessi *et al.*, 2000). Arg88 and Phe143 were also observed near this site (Fig. 4), but were not conserved in ALDH (Fig. 2). Further, no sequence homology at this site was observed between ALDH*St* and ALDH*Ps*. This may be related to the difference in substrate specificity.

3.3. Structure and thermostability of ALDH*St*

Enzyme thermostability can be achieved through several structural features controlled by hydrogen bonds, salt bridges, hydrophobic interactions, proline residues or disulfide bridges. Among these, many salt bridges have been observed on the surface of hyperthermophilic enzymes (Arnott *et al.*, 2000; Christodoulou *et al.*, 2003; Tanaka *et al.*, 2006). The number of arginine residues in ALDH*St* and ALDH*Ps* was determined to be 27 and 32, respectively. Generally, the side chains of arginine residues are involved in the formation of salt bridges on the enzyme surface. In this study, we identified several unique arginine residues in ALDH*St*. In the cofactor-binding

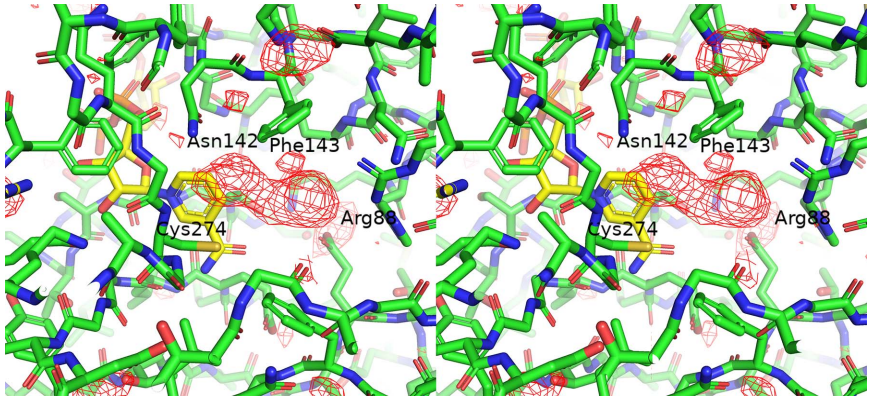

Figure 4
Cross-eyed stereo figure of the conformation of the active-site residue Asn142 in ALDH*St*. The coenzyme (NADP) is shown in yellow. The omit $F_o - F_c$ electron-density map for the holo model of ALDH*St* is contoured at 3σ and colored red.

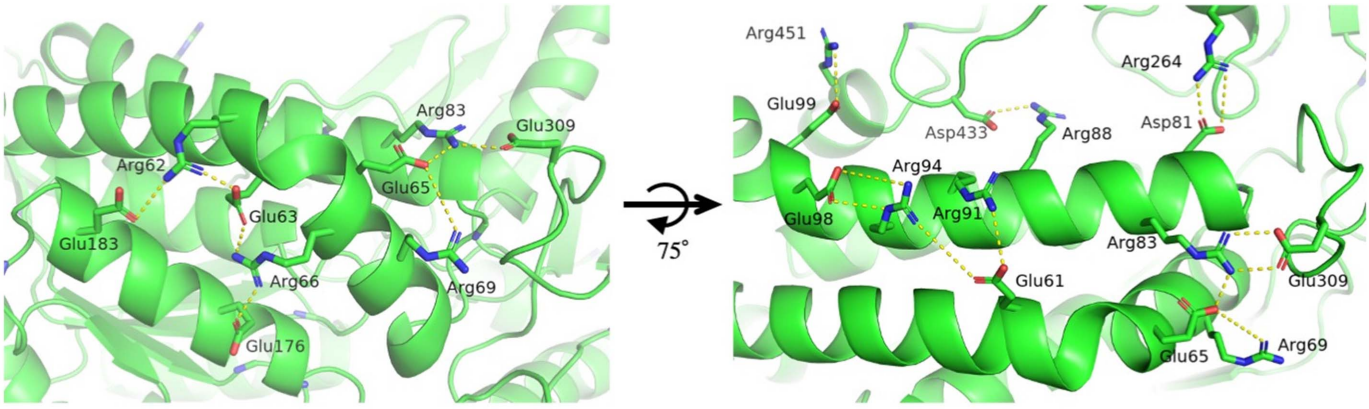

Figure 5
The surface structure of the α-helices in the cofactor-binding domain of ALDH*St*. Arg, Glu and Asp residues involved in salt bridges are shown as stick models with the interactions shown as dashed lines on the α-helix structures in the cofactor-binding domain of ALDH*St*.

domain of ALDH*St*, many salt-bridge networks between Arg and Glu/Asp are observed on the surface of the three α-helices (Fig. 5). Thus, the number of arginine residues may correlate with the thermostability of ALDH.

4. Conclusion

The crystal structure of thermostable acetaldehyde dehydrogenase from *S. tokodaii* was determined in the holo form. This structural information provides clues regarding the mechanisms of substrate recognition and hyperthermostability in ALDH.

Acknowledgements

X-ray diffraction data were obtained using beamline BL44XU at SPring-8, Hyogo, Japan with the approval of the Institute for Protein Research, Osaka University, Osaka, Japan (Proposal Nos. 2018A6851, 2018B6851, 2019A6951, 2019B6951, 2020A6550, 2021A6641 and 2021B6641).

Funding information

This work was supported by a private fund from Rakuto Kasei Industrial Co. Ltd, Shiga, Japan.

References

Arnott, M. A., Michael, R. A., Thompson, C. R., Hough, D. W. & Danson, M. J. (2000). *J. Mol. Biol.* **304**, 657–668.
Bairoch, A. (2000). *Nucleic Acids Res.* **28**, 304–305.
Bezsudnova, E. Y., Petrova, T. E., Artemova, N. V., Boyko, K. M., Shabalin, I. G., Rakitina, T. V., Polyakov, K. M. & Popov, V. O. (2016). *Archaea*, **2016**, 9127857.
Christodoulou, E., Rypniewski, W. R. & Vorgias, C. R. (2003). *Extremophiles*, **7**, 111–122.
Cobessi, D., Tête-Favier, F., Marchal, S., Branlant, G. & Aubry, A. (2000). *J. Mol. Biol.* **300**, 141–152.
Demkiv, O., Smutok, O., Paryzhak, S., Gayda, G., Sultanov, Y., Guschin, D., Shkil, H., Schuhmann, W. & Gonchar, M. (2008). *Talanta*, **76**, 837–846.
Emsley, P., Lohkamp, B., Scott, W. G. & Cowtan, K. (2010). *Acta Cryst.* D**66**, 486–501.
Ishikawa, K., Higashi, N., Nakamura, T., Matsuura, T. & Nakagawa, A. (2007). *J. Mol. Biol.* **366**, 857–867.
Ishikawa, K., Ishida, H., Matsui, I., Kawarabayasi, Y. & Kikuchi, H. (2001). *Appl. Environ. Microbiol.* **67**, 673–679.
Ito, F., Chishiki, H., Fushinobu, S. & Wakagi, T. (2013). *Biosci. Biotechnol. Biochem.* **77**, 1344–1348.
Kataoka, M. & Ishikawa, K. (2014). *Biosci. Biotechnol. Biochem.* **78**, 1537–1541.
Kim, H.-W. & Ishikawa, K. (2011). *Biochem. J.* **437**, 223–230.
Kimura, M., Yokoyama, A. & Higuchi, S. (2019). *Expert Opin. Ther. Targets*, **23**, 955–966.
Liu, T., Hao, L., Wang, R. & Liu, B. (2013). *Extremophiles*, **17**, 181–190.
Lovell, S. C., Davis, I. W., Arendall, W. B., de Bakker, P. I. W., Word, J. M., Prisant, M. G., Richardson, J. S. & Richardson, D. C. (2003). *Proteins*, **50**, 437–450.
Matthews, B. W., Cohen, G. H., Silverton, E. W., Braxton, H. & Davies, D. R. (1968). *J. Mol. Biol.* **36**, 179–183.
Monkawa, A., Gessei, T., Takimoto, Y., Jo, N., Wada, T. & Sanari, N. (2015). *Sens. Actuators B Chem.* **210**, 241–247.
Murshudov, G. N., Skubák, P., Lebedev, A. A., Pannu, N. S., Steiner, R. A., Nicholls, R. A., Winn, M. D., Long, F. & Vagin, A. A. (2011). *Acta Cryst.* D**67**, 355–367.
Otwinowski, Z. & Minor, W. (1997). *Methods Enzymol.* **276**, 307–326.
Perozich, J., Nicholas, H., Wang, B.-C., Lindahl, R. & Hempel, J. (1999). *Protein Sci.* **8**, 137–146.
Tanaka, T., Sawano, M., Ogasahara, K., Sakaguchi, Y., Bagautdinov, B., Katoh, E., Kuroishi, C., Shinkai, A., Yokoyama, S. & Yutani, K. (2006). *FEBS Lett.* **580**, 4224–4230.
Vagin, A. & Teplyakov, A. (2010). *Acta Cryst.* D**66**, 22–25.
Wang, W., Wang, C., Xu, H. & Gao, Y. (2020). *Int. J. Biol. Sci.* **16**, 921–934.
Zhang, Y., Yu, Y., Zhang, C., Song, N., Guo, Z. & Liang, M. (2022). *Anal. Chem.* **94**, 15827–15831.